Theoretical analysis of absorption and resonant Raman scattering spectra of *trans*-$(CH)_x$

G. P. Brivio and E. Mulazzi
Dipartimento di Fisica dell'Università and Gruppo Nazionale, Struttura della Materia del Consiglio Nazionale delle Richerche, via Celoria 16, I-20133 Milano, Italy

(Received 28 November 1983; revised manuscript received 19 March 1984)

Detailed and fully consistent calculations of absorption and resonant Raman scattering spectra from *trans*-$(CH)_x$ have been performed by using a bimodal Gaussian distribution centered on short and long segments which form the *trans*-$(CH)_x$ chain. Such results are in good agreement with the experiments. With the use of our model it is also possible to account for several properties of *trans*-polyacetylene: the conjugation length of the segments which constitute the chain (for undoped and doped samples), isomerization processes, and the history of the sample under investigation.

I. INTRODUCTION

The study of both experimental and theoretical properties of *trans*-polyacetylene has recently attracted much scientific interest. Experiments have first been performed on magnetic and transport properties on undoped and doped samples.[1,2] Later several measurements for photoexcitations and photoconductivity in *trans*-$(CH)_x$ have been reported.[3–7] Also much information on *trans*-$(CH)_x$ properties has been gained by investigating absorption and resonant Raman scattering (RRS) spectra.[8,9] Since the optical responses strongly depend on the history of the *trans*-$(CH)_x$ films,[8] they provide an important contribution to the understanding of the morphology of the particular sample under investigation. This could be of great relevance in explaining the conducting properties of the undoped and doped systems. Line-shape analyses of Raman spectra in *trans*-$(CH)_x$ (Refs. 8–10) display the unusual feature of drastic changes both in the intensity of the two main peaks at ω_{C-C} (single bond) and at $\omega_{C=C}$ (double bond), and in the relative position of the side bands, as function of the laser exciting frequency. These bands in the first-order Raman spectra are essentially determined by the scattering from the C—C (single bond) and the C=C (double bond) stretching vibrational modes.

Different models have been considered to explain all experimental properties of *trans*-$(CH)_x$. Pople and Walmsley[11] first introduced the possibility of defects in alternation bonds in polyene chains (PW defects). Following that hypothesis, Su, Schrieffer, and Heeger[12] (SSH) have considered elementary excitations of the chain in the form of a topological soliton or moving domain wall. Such a soliton (SSH model) would require a long polyacetylene chain, and is expected to be a neutral one with an unpaired spin localized in the wall.[12] On the other hand, according to the SSH theory[12] in the case of doped samples where an electron or a hole is transferred to the chain or in a photoexcitation process in undoped *trans*-$(CH)_x$ a charged soliton with zero spin is formed.[7] By the soliton model different properties of polyacetylene (paramagnetic susceptivity, conductivity, photoconductivity, photoexcitations) are currently explained by several authors.[1–3,5–7,13] However, controversies and different interpretations exist in this area.[4,14–16]

A similar infinite chain model has also been introduced to study the Raman spectra.[17] By making the assumption that *trans*-$(CH)_x$ samples are only constituted from long chains, Mele has interpreted the high-frequency sidebands in the Raman spectra as due to a hot luminescence process.[17] Following this approach it is, however, difficult to explain the changes in the absorption and RRS spectra in terms of the history of the samples. Also, Mele predicts an increasing shift for both sidebands by increasing the laser frequency, particularly for the one associated with the 1060-cm^{-1} band (C—C stretching mode) in disagreement with the experimental data. Furthermore, by the Mele theory,[17] again in disagreement with the experimental data, the intensities of the sidebands decrease, by increasing the incident light frequency.

A different theoretical approach to the study of optical properties of *trans*-$(CH)_x$ is the simpler assumption that the sample under investigation is formed by different conjugation-length segments. Kuzmany *et al.* first suggested that the shapes of the spectra are crucially affected by the various lengths of the segments of *trans*-$(CH)_x$ and assumed that segments of different lengths are weighted according to a modified Gaussian distribution and subsequently according to a bimodal distribution.[18] But in these calculations only the short-length segments are mainly weighted and determine the whole properties of RRS and absorption of *trans*-$(CH)_x$.

In this paper, carrying on calculations on absorption and RRS spectra of *trans*-$(CH)_x$, using a model recently introduced by the authors,[10,19,20] we start from the hypothesis that both long and short segments of the chain contribute to those spectra. Such a contribution is taken into account by using a bimodal distribution determined by two normalized Gaussians—the former centered on short segments, the latter on long segments of the chains. We suppose that these *trans*-$(CH)_x$ segments of different conjugation length are formed in the chain in the cis/trans isomerization process. In this way we can account for the history of the sample. In our model the electronic and vibrational properties of these segments of

different cojungation lengths are considered to be unperturbed by the presence of defects at the end of the segment. This is justified by the fact that the electronic transitions of these defects lie in the gap between the conduction and valence bands and that the vibrations appropriate to such defects do not couple to the electronic transitions taken into account.

We summarize the main formulas on optical response functions and present a discussion on long- and short-segment electronic states, dipole moments, and electron-vibration interactions in Sec. II. In Sec. III the results of our calculations are compared with the experimental results and Sec. IV is devoted to discussion and conclusions.

II. BASIC FORMULAS

We follow the model already developed by the authors[10,20] in order to evaluate the absorption and the resonant Raman scattering spectra of *trans*-$(CH)_x$. Such a theoretical approach is based on the one-electron approximation for what concerns all the electronic transitions $\pi \rightarrow \pi^*$ and the electron vibrational interactions, taking into account the properties of these quantities for long- and short-conjugation lengths of the chain. By using a phenomenological model the change of the C—C (ω_{C-C}) and C=C ($\omega_{C=C}$) vibrational frequencies as a function of the conjugation length is considered in evaluating the optical response functions. We briefly summarize and comment on the main formulas used in our calculation.

For the absorption spectrum one has to distinguish between the long- and short-segment contributions in the response function $I(\Omega)$:

$$I(\Omega)=\sum_N [P_1(N)I_1(\Omega,N)+P_2(N)I_2(\Omega,N)] , \tag{2.1}$$

where $I_1(\Omega,N)$ and $I_2(\Omega,N)$ are the long- and short-segment absorption functions, respectively. $P_1(N)$ and $P_2(N)$ are the Gaussian weights depending on N, the number of double bonds in the segment. They are defined as

$$\begin{aligned} P_1(N)&=(2\pi\sigma_1^2)^{-1/2}\exp[-(N-N_1)^2/2\sigma_1^2]G , \\ P_2(N)&=(2\pi\sigma_2^2)^{-1/2}\exp[-(N-N_2)^2/2\sigma_2^2](1-G) . \end{aligned} \tag{2.2}$$

The number $0 \le G \le 1$ weights the normalized Gaussians. N_1 and N_2 are the most probable double-bond numbers for long and short segments of the chain, with σ_1 and σ_2 their respective standard deviations.

For $N > 30$ one defines

$$I_1(\Omega,N)=\frac{\Omega}{N}\sum_{j=0}^{1}\sum_{i=1}^{2}\sum_{-\pi/a\le k\le\pi/a} |M_k|^2 \exp\left[-\sum_{i=1}^{2} V_{k,i}\right](V_{k,i})^j \frac{\gamma}{(\Omega-\Omega_k-j\omega_{iN})^2+\gamma^2} . \tag{2.3}$$

For $4 \le N < 30$,

$$I_2(\Omega,N)=\Omega\sum_{j=0}^{1}\sum_{i=0}^{2}\sum_{n=1}^{N} |M_n|^2 \exp\left[-\sum_{i=1}^{2} V_{n,i}\right](V_{n,i})^j \frac{\gamma}{(\Omega-\Omega_n-j\bar{\omega}_{iN})^2+\gamma^2} . \tag{2.4}$$

Before explaining Eqs. (2.3) and (2.4) with some detail we introduce the first-order RRS cross section, where the long- and short-segment contributions are taken into account in the same way as in Eq. (2.1):

$$\frac{d^2\sigma}{d\phi\, d\omega} \propto \sum_N \sum_{s=1}^{2} [P_1(N)S_{1,s}(\omega,\Omega_L,N)+P_2(N)S_{2,s}(\omega,\Omega_L,N)] . \tag{2.5}$$

In Eq. (2.5) the sum over s takes into account the total contribution of both vibrational frequencies ω_{C-C} and $\omega_{C=C}$ to the RRS spectra. $P_1(N)$ and $P_2(N)$ are the same Gaussian weights as in Eq. (2.2). Ω_L is the frequency of incident light. $S_{1,s}(\omega,\Omega_L,N)$ and $S_{2,s}(\omega,\Omega_L,N)$ are the contributions to first-order RRS from long and short segments, respectively. Their expressions are given by the following. For $N \ge 30$,

$$\begin{aligned} S_{1,s}(\omega,\Omega_L,N)=(\Omega_L-\omega_{sN})^3\Omega_L \frac{1}{N} \sum_{-\pi/a\le k\le\pi/a} |M_k|^4 V_{k,s} \left|\sum_{l=0}^{1}(-1)^l R_1(\Omega_L-\Omega_k-l\omega_{sN})\right|^2 (2\pi\Delta_N^2)^{-1/2} \\ \times \exp\left[-\frac{(\omega-\omega_{sN})^2}{2\Delta_N^2}\right] , \end{aligned} \tag{2.6}$$

where

$$R_1(\Omega_L-\Omega_k)=\exp\left[-\sum_{i=1}^{2} V_{k,i}\right]\sum_{j=0}^{1}\sum_{i=1}^{2}(V_{k,i})^j \frac{\gamma+i(\Omega_L-\Omega_k-j\omega_{iN})}{\gamma^2+(\Omega_L-\Omega_k-j\omega_{iN})^2} . \tag{2.7}$$

For $4 \le N < 30$,

$$S_{2,s}(\omega,\Omega_L,N)=(\Omega_L-\bar{\omega}_{sN})^3\Omega_L \sum_{n=1}^{N} |M_n|^4 V_{n,s} \left|\sum_{l=0}^{1}(-1)^l R_2(\Omega_L-\Omega_N-l\bar{\omega}_{sN})\right|^2 (2\pi\bar{\Delta}_N^2)^{-1/2} \exp\left[-\frac{(\omega-\bar{\omega}_{sN})^2}{2\bar{\Delta}_N^2}\right] , \tag{2.8}$$

$$R_2(\Omega_L-\Omega_N)=\exp\left[-\sum_{i=1}^{2}V_{n,i}\right]\sum_{j=0}^{1}\sum_{i=1}^{2}(V_{n,i})^j\frac{\gamma+i(\Omega_L-\Omega_n-j\omega_{iN})}{\gamma^2+(\Omega_L-\Omega_n-j\bar{\omega}_{iN})^2}\ . \tag{2.9}$$

In all formulas (2.3), (2.4), (2.6), (2.7), (2.8), and (2.9) the index j labels the zero- and one-phonon processes, the index i refers to the two vibrational modes of the chain ω_{C-C} ($i=1$), and $\omega_{C=C}$ ($i=2$), with frequency ω_{iN} (depending on N) for long segments and $\bar{\omega}_{iN}$ for short segments. γ represents one-half of the reciprocal of the lifetime of the electronic excited states. For the sake of simplicity we do not take into account any N dependence of γ. So the same value for γ is used in evaluating the long- and short-segment contributions to Eqs. (2.1) and (2.3)—(2.9). In Eqs. (2.6) and (2.8) Δ_N and $\bar{\Delta}_N$ are the widths of the Raman scattering line shape for each vibrational frequency ω_{sN} and $\bar{\omega}_{sN}$.

In Eqs. (2.3), (2.6), and (2.7) the Born—von Kármán condition is used for electronic wave functions, which are Bloch waves, and k represents their wave vectors. The allowed values of k depend on N (number of double bonds). Ω_k and M_k are the vertical electronic transition frequencies and relative electric dipole moments, whose expressions are given in Refs. 20—22. For long segments M_k are parallel to the axis of the chain. In Eqs. (2.3), (2.6), and (2.7)

$$V_{k,i}=(V_{e\text{-ph};k,i}/\omega_{iN})^2\ , \tag{2.10}$$

where $V_{e\text{-ph};k,i}$ is the linear interaction between the electronic excited state and the C—C and C=C vibrational modes ($i=1,2$), respectively, for $q\simeq 0$, projected on the axis of the chain. For long segments ($N\geq 30$) one can show that the two interactions $V_{e\text{-ph};k,i}$ considered here, projected on the axis of the chain are almost of equal intensity. Then $V_{k,i}$ is depending on ω_{iN} as shown in Eq. (2.10). In fact for all the Ω_k that we consider here, the electron-vibration interactions can be written[10,21]

$$V_{e\text{-ph};k,i}\simeq\frac{\delta\beta_2}{\delta R_2}\frac{(1+\nu\cos\theta)}{(1+\nu^2+2\nu\cos\theta)^{1/2}}\ ; \tag{2.11}$$

β_2 and $\beta_1=\nu\beta_2$ are the hopping integrals on the double and single bonds, respectively, along the chain; $\theta=ka$ (a is the unit cell length, and δR_1 and δR_2 are the displacements from the equilibrium configuration on single and double bonds). $\delta\beta_2/\delta R_2$ can be evaluated from Ref. 23, and we assume as previously

$$\frac{V_{k,1}}{V_{k,2}}\sim\left[\frac{\omega_{2N}}{\omega_{1N}}\right]^2\simeq 1.6\ .$$

This result, which is valid at $q\simeq 0$ can also be found out from the detailed calculations of the electron-vibration interactions, starting from the exact formulas taking into account lattice dynamics eigenvectors, the internal coordinates, and the variations $\delta\beta_1/\delta R_1, \delta\beta_2/\delta R_2$, as in Ref. 24. Such a point is discussed in Ref. 21.

The expressions used in the calculation for ω_{1N} and ω_{2N} are

$$\omega_{1N}=\left[1060+\frac{D}{N^2}\right]\ \text{cm}^{-1}\ , \tag{2.12}$$

$$\omega_{2N}=\left[1450+\frac{D}{N^2}\right]\ \text{cm}^{-1}\ , \tag{2.13}$$

where $D=1.5\times 10^4\ \text{cm}^{-1}$. Equations (2.12) and (2.13) which express the phonon dispersion relationship of the two frequencies for $q=0$ in a qualitative way (see, for instance, Ref. 25), have to be considered, since they account for the phonon density of states near the critical point at $q\simeq 0$. This implies that the electron-vibration interactions for long segments must be weighted by such a phonon density of states.

We discuss now the physical quantities which enter formulas (2.4), (2.8), and (2.9) to calculate the absorption and RRS spectra for short segments.

The electronic eigenvectors, and eigenvalues are obtained by diagonalizing a one-electron Hückel matrix of dimension $2N$ (N being the number of double bonds),[26] which neglects wave-function overlap and only considers hopping terms between nearest neighbors. For the electronic dipole moments $M_{ge}(N)$, we use the following expression:

$$M_{ge}(N)=\sum_{r,r'}d_{rr'}c_{rg}(N)c_{r'e}(N)\delta_{r',r\pm 1}\ . \tag{2.14}$$

We stress that the indices g and e refer to one-electron states in the total ground and excited electronic state. $d_{rr'}$ independent of N, are the atomic dipole moments calculated with respect to the π-electronic wave function of nearest-neighbor C atoms, which we assume independent of the position in the segment, labeled with r and r'. $\{c_{rg}(N)\}$ and $\{c_{r'e}(N)\}$ are the real eigenvector solutions of the Hückel problem for electronic ground (g) and excited states (e). In this model the dipole moment matrix $M_{ge}(N)$ is an N-dimensional one, whose row and column indices g and e, running from 1 to N, label all one-electron states in the ground and excited states, respectively, with increasing energy. By computing the matrix elements of $M_{ge}(N)$ from formula (2.14), one can see that those appreciably different from zero are the diagonal ones and we can rewrite the matrix $M_{ge}(N)$ simply as an N-dimensional vector $M_n(N)\equiv M_n$ with n running from the lowest-energy difference between excited and ground states. Formally $n=e\delta_{e,N-g+1}$. For the same reason in formulas (2.4), (2.8), and (2.9), $\Omega_n(N)\equiv\Omega_n$ function of the double-bond number N in the segment, are the corresponding electronic transition frequencies between ground and excited states. In Fig. 1 we report the computed results for M_1 and M_2, as a function of the number of double bonds N, which show an increase with N, and saturation at $N\geq 30$.

In the framework of the Hückel model and in the deformation potential approximation we have computed the electron-vibration couplings in the electronic excited states of frequencies Ω_n with respect to the ground state, for any N, in the following way:

$$V_{n,i}(N)\equiv V_{n,i}=(V_{e\text{-ph};n,i}(N)/\bar{\omega}_{iN})^2\ , \tag{2.15}$$

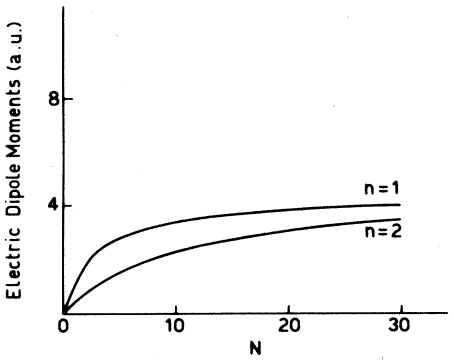

FIG. 1. Calculated electric dipole moments for $n=1$ (M_1) and $n=2$ (M_2) as a function of N, number of double bonds. The values are expressed in arbitrary units (a.u.).

$$V_{e\text{-ph};n,i}(N)=\sum_{r,r'} U_{i;rr'}(N)c_{rn}(N)c_{r'n}(N)\delta_{r',r\pm1} \ . \qquad (2.16)$$

In formula (2.16) $U_{i,rr'}(N)$ depends, in an analogous way as for the electron-vibration interaction for long segments, on the eigenvectors of the stretching normal modes and on $\delta\beta_1/\delta R_1, \delta\beta_2/\delta R_2$, evaluated for short segments with N double bonds. Then in principle one has to evaluate the lattice dynamics of the finite segments in order to solve the eigenvalue problem and to calculate the eigenvectors to introduce in Eq. (2.16). Furthermore, since the electron-vibration interaction is projected onto the electric dipole moments of the segments and depends on the product $c_{nr}(N)c_{nr'}(N)$ of the excited state electronic eigenvectors [see Eq. (2.16)], one has to consider the change in delocalization on the double and single bonds of the electric dipole moments and of the product $c_{nr}(N)c_{nr'}(N)$ going from segments with $N=30$ to segments with $N=4$.

We give in Fig. 2 the dependence of $V_{1,i}$ ($i=1,2$, $n=1$) as a function of $1/N$, that we have considered in the present calculations. In order to obtain that dependence, we use the following input data: at $N=30$ the values obtained for long segments, at $N=11$ the values obtained by using the lattice dynamics data for the stretching modes of β-carotene in Ref. 27, and for the electronic part the values obtained by solving the corresponding Hückel problem. For $4\leq N<6$ we use the phenomenological law obtained from the data of Ref. 28. The electron-vibration couplings $V_{n,i}(N)$ for $n=1$ are scaled from the values given in Fig. 2 by a factor calculated from the product $c_{rn}(N)c_{r'n}(N)$. We stress that, differently from our previous calculations for short segments,[10,20] where we only took into account the lowest-energy electronic transition ($n=1$), for each N (number of double bonds) in this paper all possible electronic transitions with frequency $\Omega_n \leq 4$ eV, from the ground to the excited state, are considered. For this reason a summation on index n is introduced in Eqs. (2.4) and (2.8), because the dipole moments and the electron-vibration interaction terms depend on n.

All the parameters introduced in our model for the calculation of the electronic and vibrational properties of *trans*-$(CH)_x$ for short segments, are chosen in such a way as to smoothly connect all the corresponding physical

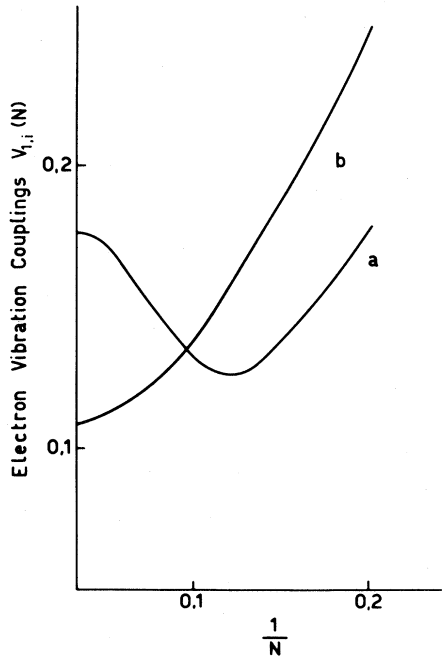

FIG. 2. Calculated electron-vibrational coupling $V_{1,i}$ for the first excited electronic state for $i=1,2$ as a function of $1/N$. Curve a refers to $V_{1,1}$; curve b refers to $V_{1,2}$.

quantities (frequencies, dipole moments, electron-vibration interactions) to those of long segments at $N=30$. More precisely, for a good fit with absorption and RRS experimental data, the values for the hopping integrals, $\beta_1\equiv\beta_1(N)$ and $\beta_1\equiv\beta_1(N)$ [defined from $\beta_1=\nu\beta_2$, with $\nu\equiv\nu(N)$] used in the Hückel matrix, decrease by increasing N in the interval $4\leq N\leq 30$, from the values $\beta_2(4)=4.18$ eV and $\beta_1(4)=3.453$ eV to $\beta_2(30)=3.25$ eV and $\beta_1(30)=2.356$ eV. At $N=30$ both hopping integrals β_2 and β_1 merge to the long-segment constant values, which are valid for $N\geq 30$. The ratios ν decrease linearly from the values $\nu(4)=0.85$ to $\nu(25)=0.725$, and keep constant in the interval $25\leq N\leq 29$. So, as we have chosen the values of β_2 to decrease linearly with increasing N, the values of β_1 decrease more rapidly in the interval $4\leq N\leq 24$ and then linearly in the interval $25\leq N\leq 29$. This hypothesis expresses the usual properties of larger hopping for shorter segments, and lower ratio ν for larger segments of the polyenes.[26]

Also, the formulas that we use for the $\bar{\omega}_{iN}$ are

$$\bar{\omega}_{1N}=\left[1060+\frac{B_1}{N}\right]\ \text{cm}^{-1}\ ,$$
$$\bar{\omega}_{2N}=\left[1450+\frac{B_2}{N}\right]\ \text{cm}^{-1}\ , \qquad (2.17)$$

where $B_1=600\ \text{cm}^{-1}$ and $B_2=500\ \text{cm}^{-1}$.

We want to draw the reader's attention to the important point that the electron-vibration interaction matrix elements entering Eqs. (2.11) and (2.16), $V_{e\text{-ph};k,i}$ and $V_{e\text{-ph};n,i}(N)$, respectively, are calculated in the excited electronic states relative to long- and short-conjugation

segments. Such expressions are completely different from the electron-vibration interaction matrix elements (even if they all depend on $\delta\beta_1/\delta R_1$ and $\delta\beta_2/\delta R_2$; see also Ref. 24) entering the correction to the dynamical matrix δL as described in Ref. 25 for long segments and analogously applicable to the dynamical matrix correction for short segments. In fact, in the expression δL, matrix elements only appear which mix ground and excited electronic states. Since this expression[25] depends on the inverse of the transition frequencies from the ground to the excited states (which increase as a function of k, starting from $k=\pm\pi/a$, for long segments, and of $1/N$ for short segments) and on the mixing matrix elements (which decrease as function of k and q for long segments and on $1/N$ for short segments), it is trivial to show that the δL correction decreases as a function of q and $1/N$, respectively.

So the stretching vibrational frequencies evaluated in the Hückel approximation[25] are consistent with the experimental data which show increasing frequencies by increasing q and $1/N$. Then the phenomenological formula which we use for long- and short-segment vibrational frequencies [Eqs. (2.12), (2.13), and (2.17)] are in order with this approximation and with the experimental data. On the other hand, the electron-vibration interaction matrix elements entering the electron-vibration couplings shown in Fig. 2 are evaluated in the excited electronic states and present a different behavior from the mixing matrix elements entering δL, as a function of $1/N$ as previously discussed and as shown in Fig. 2. Then as a consequence, in the Hückel approximation, the electronic transition frequencies, the stretching mode vibration frequencies relative to the ground state, and the electron vibration couplings in the excited electron states *all increase* as a function of $1/N$, in the same consistent model.

III. COMPUTED ABSORPTION AND RRS SPECTRA

The parameters used in calculation for the absorption and RRS spectra which enter formulas (2.1)–(2.17) of our model are the following: $N_1=100$, $\sigma_1=50$, $N_2=15$, $\sigma_2=7$, $G=0.75$, $\gamma=0.1$ eV, $\Delta_N=12$ cm^{-1}, and $\overline{\Delta}_N=(12+40/N)$ cm^{-1}. The absorption and RRS spectra that we report take into account all possible electronic transitions of frequency $\Omega_n \leq 4$ eV.

In Fig. 3 we show the absorption spectrum given by formulas (2.1)–(2.3). This is in good agreement with the experimental results of Ref. 29. It displays a principal peak due to the long-segment transition frequencies at $\Omega=1.833$ eV. The tail for higher frequencies is determined by the electronic transitions of shorter segments.

In Fig. 4 we report the RRS spectra due to the single- and double-stretching modes $\omega_{C-C}=1060$ and $\omega_{C=C}=1450$ cm^{-1}, respectively. The resonant laser scattering excitation frequencies Ω_L are listed therein. As one can see from Fig. 4, where we also present the experimental data from Ref. 9, by varying the incident light frequency, the line shapes of the two peaks centered at ω_{C-C} and $\omega_{C=C}$ change in agreement with the experimental results. Moreover, the intensity ratio of the two peaks at 1060 and 1450 cm^{-1} varies. In Fig. 5 we report the RRS spectra

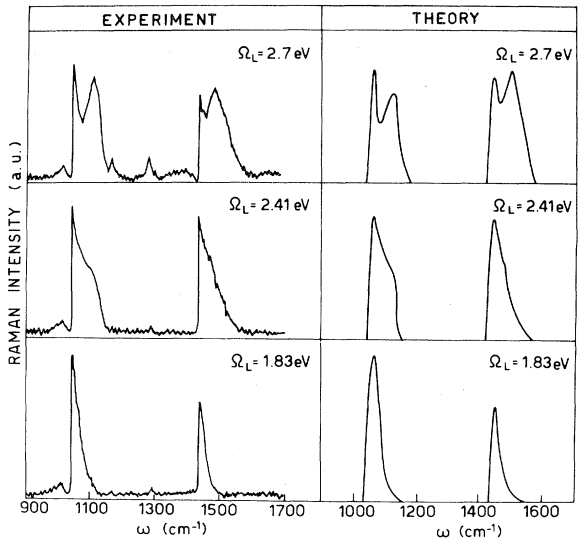

FIG. 4. Experimental and calculated RRS spectra of *trans*-$(CH)_x$ for different incident light frequencies Ω_L as listed therein. The experimental data are taken from Ref. 10. The parameters used for the calculations are the same as in Fig. 3.

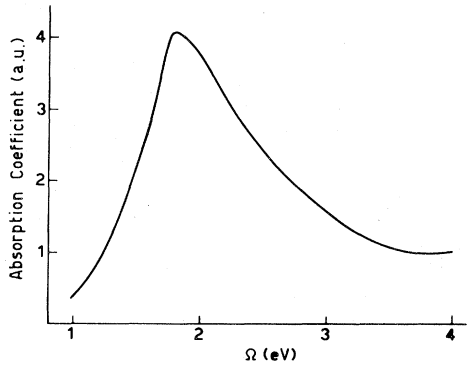

FIG. 3. Calculated absorption spectrum of *trans*-$(CH)_x$. The parameters are given in the text.

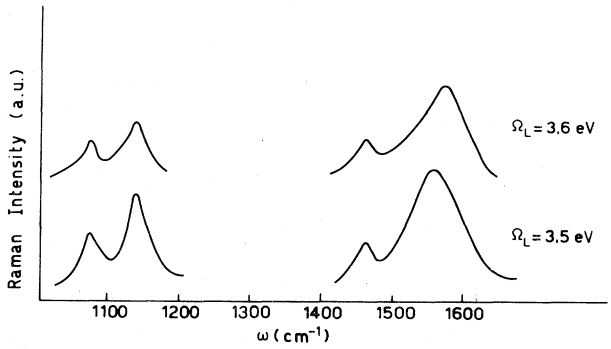

FIG. 5. Calculated RRS spectra of *trans*-$(CH)_x$ for different incident light frequencies Ω_L as listed therein. The parameters are the same as in Figs. 3 and 4.

calculated for $\Omega_L \geq 3.5$ eV. We would like to note that while the intensity and the frequency of the sideband for the RRS spectrum centered at 1450 cm^{-1} both increase, upon increasing the laser frequency for $\Omega_L \geq 3.5$ eV the frequency of the sideband of the peak centered at 1060 cm^{-1} does not change appreciably for $\Omega_L \geq 3.5$ eV. In this latter case the intensity of the second peak, however, still increases. This agrees with the experimental data in Refs. 9 and 10. Such a behavior of RRS spectra shown in Figs. 4 and 5 is due to the interplay between the resonance condition in the electronic transition frequencies of long and short segments which form the *trans*-$(CH)_x$ chain and the electron-vibration interaction, whose properties are expressed in formula (2.11), for long segments and in Fig. 2 for short segments. It is clear from Figs. 4 and 5 that the changes in the shape of the bands of the RRS spectra for larger and larger incident light frequency are due to the resonance condition with the electronic transitions of shorter and shorter segments. Therefore, our interpretation of RRS spectra require considering both long and short segments in the chain, whose percentual weight of long segments G is crucial in interpreting the experimental results. By decreasing G (which means increasing the weight of short segments) the calculated RRS spectra change and could explain why *trans*-$(CH)_x$ RRS experimental results depend on the history of the sample.

In order to show this effect, in Fig. 6 we present the calculations that we have performed, by using the model discussed in this paper, to fit the RRS spectra of Ref. 30 obtained at different isomerization times from *cis*- to *trans*-$(CH)_x$ at $T = 102\,^{\circ}C$ and for $\Omega_L = 2.7$ eV. In Fig. 6 we display the change of the line shape of the single-bond stretching frequency ω_{C-C} for increasing isomerization times. The parameters used are, for line shape a, $N_1 = 20$, $N_2 = 10$, $\sigma_1 = 10$, $\sigma_5 = 5$, $G = 0.3$; for line shape b, $N_1 = 50$, $N_2 = 10$, $\sigma_1 = 20$, $\sigma_2 = 5$, $G = 0.4$; for line shape c, $N_1 = 100$, $N_2 = 15$, $\sigma_1 = 50$, $\sigma_2 = 7$, $G = 0.7$. All other parameters used in the calculations of such spectra are unchanged with respect to those introduced to calculate the spectra of Figs. 4 and 5.

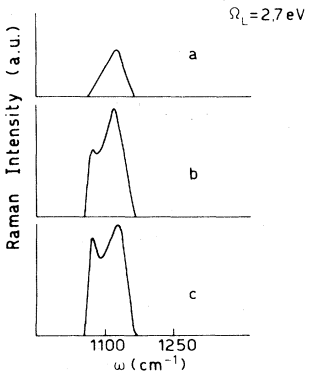

FIG. 6. Calculated RRS spectra for incident laser frequency $\Omega_L = 2.7$ eV during the isomerization process. Line shape a refers to the experimental results of Ref. 30 obtained with isomerization times $t = 30$ min, line shape b with $t = 960$ min, and line shape c with $t = 7680$ min. The parameters are given in the text.

First we want to point out that the RRS spectrum from the completely isomerized sample (curve c) and Ref. 30 is slightly different from that of Fig. 4 and Ref. 10 (obtained with the same incident laser frequency $\Omega_L = 2.7$ eV) since this latter spectrum[10] is obtained from a better quality sample. This is experimentally evidenced by the lower intensity of the sideband of the single-bond stretching mode frequency and theoretically by a slightly higher value of G ($G = 0.75$ for Fig. 4 with respect to $G = 0.7$ for line shape c). In fact as pointed out in Ref. 30 the higher the temperature, the faster the isomerization process and better quality samples are obtained. Second, as already discussed in Ref. 30 these RRS spectra can be interpreted by considering that at the beginning of the isomerization process the short-conjugation length segments are present at a higher percentage with respect to the long ones; this percentage varies during the isomerization process and at the end the long ones are more numerous than the short ones.

In the same manner, by changing the parameters N_1 and N_2 and G so that by increasing the weight of the short segments, in the calculations of RRS spectra, we can fit all the available experimental RRS data from poor quality samples (see, for instance, Ref. 31). Very poor quality samples are characterized, for incident laser frequency $\Omega_L = 2.7$ eV, by RRS spectra where the sidebands, with respect to the principal peaks at ω_{C-C} and $\omega_{C=C}$, are predominant, and broaden in such a way as to include the principal peaks, due to the long-segment contribution, as small shoulders at lower frequency.

IV. CONCLUSIONS AND DISCUSSION

We would like first to stress the main new points of our model for calculating RRS and absorption spectra.

(i) With respect to our first results,[10,20] all input parameters have been slightly varied. This is because we have considered all possible electronic transitions of frequency $\Omega_n \leq 4$ eV from the ground to the excited state, and made explicit the dependence on N (number of double bonds in the segment) of all hopping integrals (β_1 and β_2).

(ii) We were the first to calculate the interactions between the excited electronic states and the vibrational stretching modes for long segments and to introduce the N dependence of these interactions, taking into account the lengths of the segments, in order to explain the change in the line shapes in the RRS spectra.[10,20,21] Here we treat such interactions with more physical insight, and we include in the calculations also the electron-vibration interactions for all the electronic excited states with transition frequencies $\Omega_n \leq 4$ eV. All these points are not considered in Ref. 18.

(iii) We have computed the change of the line shapes of RRS spectra for different incident light frequencies Ω_L, not only for the C=C stretching modes,[10,20] but also for the C—C stretching modes. We account also for the change in the intensity ratio of the principal peaks and the position and the relative intensity of their sidebands.

The main discrepancy between our model and that of Ref. 18 lies in the treatment of the electron-vibration coupling, as just discussed, and in the choice of the distribution of chain lengths. In fact, in the calculation of RRS

reported there, 50% of the segments measure less than 15 double bonds long, while our calculations take into account that 75% of the segments are more than 30 double bonds long, with an average value of the segment length at 100 double bonds.

We have applied the same model to the evaluation of RRS spectra from *trans*-$(CD)_x$ and the results are in good agreement with the experimental data of Ref. 31. The same model, after changing N_1, N_2, σ_1, σ_2, and G, can account for RRS spectra of the sample under investigation, during the isomerization process from *cis*-$(CH)_x$ to *trans*-$(CH)_x$, and of doped *trans*-$(CH)_x$ samples.[21]

With reference to doped and undoped *trans*-$(CH)_x$ since in Ref. 7 it was suggested that the photoinduced charged soliton presents a similar IR spectrum as that created by doping, this implies equivalent dynamical properties for both charged solitons of different origin. However, following this hypothesis, it may be difficult to explain why the RRS spectra of doped systems display the sideband peak at a different frequency from that arising from an undoped system, when the spectra are obtained with the same exciting laser frequency.[8,9] On the contrary, these experimental results on RRS could suggest that no interaction between the excited electron and vibrational modes induced by the charged soliton exists. On the other hand, since it is straightforward to explain the RRS properties of undoped and doped *trans*-$(CH)_x$ systems with our theory,[32] this could draw us to the conclusion that the relevant properties of RRS spectra depend on the interactions between the excited electronic state with the stretching vibrations of long and short segments of the chain.

ACKNOWLEDGMENTS

This work was partially supported by Progetto Finalizzato Chimica Fine e Secondaria del Consiglio Nazionale delle Ricerche. One of us (G.P.B.) is grateful to Professor J. Koutecký for useful discussions on the Hückel model, and to Dr. E. Hass for permission to use his diagonalization routine.

[1]B. R. Weinberger, J. Kaufer, A. J. Heeger, A. Pron, and A. G. MacDiarmid, Phys. Rev. B 20, 223 (1979).
[2]Y. W. Park, A. Denestein, C. K. Chiang, A. J. Heeger, and A. C. MacDiarmid, Solid State Commun. 29, 747 (1979).
[3]S. Etemad, T. Mitani, M. Ozaki, T. C. Chung, A. J. Heeger, and A. G. MacDiarmid, Solid State Commun. 40, 75 (1981).
[4]H. Kiess, R. Keller, D. Baeriswyl, and G. Harbeke, Solid State Commun. 44, 1443 (1982).
[5]Z. Vardeny, J. Strait, D. Moses, T. C. Chung, and A. J. Heeger, Phys. Rev. Lett 49, 1657 (1982).
[6]B. R. Weinberger, Phys. Rev. Lett. 50, 1693 (1983).
[7]G. B. Blanchet, C. R. Fincher, T. C. Chung, and A. J. Heeger, Phys. Rev. Lett. 50, 1938 (1983).
[8]D. B. Fitchen, Mol. Cryst. Liq. Cryst. 83, 95 (1982).
[9]S. Lefrant, J. Phys. (Paris) Colloq. 44, C3-247 (1983).
[10]E. Mulazzi, G. P. Brivio, E. Faulques, and S. Lefrant, Solid State Commun. 46, 851 (1983).
[11]J. A Pople and J. H. Walmsley, Mol. Phys. 5, 15 (1962).
[12]W. P. Su, J. R. Schrieffer, and A. J. Heeger, Phys. Rev. B 22, 2099 (1980); B 28, 1138(E) (1983).
[13]S. Kivelson, Mol. Cryst. Liq. Cryst. 77, 65 (1981).
[14]S. Roth, K. Ehinger, K. Menke, M. Peo, and R. J. Schweizer, J. Phys. (Paris) Colloq. 44, C3-69 (1983).
[15]Y. Tomkiewicz, T. D. Schultz, M. B. Brom, A. R. Taranko, T. C. Clarke, and G. B. Street, Phys. Rev. B 24, 4348 (1981).
[16]G. Zerbi and G. Zannoni, J. Phys. (Paris) Colloq. 44, C3-273 (1983).
[17]E. J. Mele, Solid State Commun. 44, 827 (1982); Phys. Rev. B 26, 6901 (1982).
[18]H. Kuzmany, Phys. Status Solidi B 97, 521 (1980); H. Kuzmany, E. A. Imhoff, D. B. Fitchen, and A. Sarhangi, Phys. Rev. B 26, 7109 (1982).
[19]L. Piseri, R. Tubino, E. Mulazzi, and G. Dellepiane, in *Proceedings of the 8th ICOR, Bordeaux, 1982,* edited by J. Lascombe and P. V. Huong (Wiley, New York, 1981), p. 581.
[20]G. P. Brivio and E. Mulazzi, Chem. Phys. Lett. 95, 555 (1983); J. Phys. (Paris) Colloq. 44, C3-261 (1983).
[21]E. Mulazzi and G. P. Brivio, Mol. Cryst. Liq. Cryst. 105, 233 (1984).
[22]C. Cojan, G. P. Agrawal, and C. Flytzanis, Phys. Rev. B 15, 909 (1977).
[23]T. Kakitani, Prog. Theor. Phys. 51, 656 (1974).
[24]E. Mulazzi, R. Tiziani, and R. Tubino (unpublished).
[25]M. J. Rice and E. J. Mele, Solid State Commun. 35, 487 (1980).
[26]J. N. Murrell, *The Theory of the Electronic Spectra of Organic Molecules* (Methuen, London, 1963).
[27]Fuyuhiko Inagaki, Mitsuo Tasumi, and Tatsuo Miyazawa, J. Raman Spectrosc. 3, 335 (1975).
[28]M. F. Granville, B. E. Kohler, and J. Bannon Snow, J. Chem. Phys. 75, 3765 (1981).
[29]M. Tanaka, A. Watanabe, and J. Tanaka, Bull. Chem. Soc. Jpn. 53, 3430 (1980); L. Lauchlan, S. Etemad, T. C. Chung, A. J. Heeger, and A. C. MacDiarmid, Phys. Rev. B 24, 3701 (1981).
[30]E. A. Imhoff, Ph.D. thesis, Cornell University, 1983 (unpublished).
[31]L. S. Lichtmann, Ph.D. thesis, Cornell University, 1983 (unpublished).
[32]S. Lefrant, E. Faulques, E. Mulazzi, and G. P. Brivio (unpublished).